LETTERS

Half-metallic graphene nanoribbons

Young-Woo Son[1,2], Marvin L. Cohen[1,2] & Steven G. Louie[1,2]

Electrical current can be completely spin polarized in a class of materials known as half-metals, as a result of the coexistence of metallic nature for electrons with one spin orientation and insulating nature for electrons with the other. Such asymmetric electronic states for the different spins have been predicted for some ferromagnetic metals—for example, the Heusler compounds[1]—and were first observed in a manganese perovskite[2]. In view of the potential for use of this property in realizing spin-based electronics, substantial efforts have been made to search for half-metallic materials[3,4]. However, organic materials have hardly been investigated in this context even though carbon-based nanostructures hold significant promise for future electronic devices[5]. Here we predict half-metallicity in nanometre-scale graphene ribbons by using first-principles calculations. We show that this phenomenon is realizable if in-plane homogeneous electric fields are applied across the zigzag-shaped edges of the graphene nanoribbons, and that their magnetic properties can be controlled by the external electric fields. The results are not only of scientific interest in the interplay between electric fields and electronic spin degree of freedom in solids[6,7] but may also open a new path to explore spintronics[3] at the nanometre scale, based on graphene[8–11].

When a single graphite layer is terminated by zigzag edges on both sides, which we refer here to as a zigzag graphene nanoribbon (ZGNR) (Fig. 1), there are peculiar localized electronic states at each edge[12,13]. These edge states (which are extended along the edge direction) decay exponentially into the centre of the ribbon, with decay rates depending on their momentum[12–15]. Such states have been observed in monoatomic step edges of graphite by using scanning probe techniques[16,17]. The localized edge states form a twofold degenerate flat band at the Fermi energy (E_F), existing in about one-third of the Brillouin zone away from the zone centre[12–15]. By invoking band ferromagnetism, it has been suggested that an opposite spin orientation across the ribbon between ferromagnetically ordered edge states on each edge in ZGNRs is the ground-state spin configuration; that is, the total spin is zero[12,18,19]. Because the states around E_F are the edge states and linear combinations of them, the effects of external transverse fields are expected to be significant on these states, in contrast with those on the extended states[20].

Our study of the spin-resolved electronic structure of ZGNRs is based on the *ab initio* pseudopotential density functional method[21] within the local spin density approximation[22]. A periodic saw-tooth-type potential perpendicular to the direction of the ribbon edge is used to simulate the external electric fields (E_{ext}) in a supercell (Fig. 1). In accordance with previous convention[12–15], the ZGNRs are classified by the number of zigzag chains (n; Fig. 1) forming the width of the ribbon. We will hereafter refer to an ZGNR with n zigzag chains as an n-ZGNR. When the spin degree of freedom is neglected, our calculation from first principles also predicts a twofold degenerate flat band at E_F (Fig. 2a). But the spinless state is not the ground state. Moreover, the electronic structures of the ZGNRs show marked alterations when spins and E_{ext} are included.

Considering first the spin degree of freedom, we find as in previous studies that the configuration with opposite spin (antiferromagnetic) orientation between ferromagnetically ordered edge states at each edge (Fig. 2b) is favoured as the ground state over the configuration with same spin orientation between the two edges[12,18,19] (The present result of antiferromagnetic spin configuration on the honeycomb lattice is consistent with a theorem for electrons on a bipartite lattice[23].) Our calculations show that the magnetic interaction energies are quite large. For example, the total energy difference between a spin-polarized edge and a spin-unpolarized one is 20 meV per edge atom for 8-ZGNR, and the spin configuration is further stabilized by 2.0 meV per edge atom as a result of the antiferromagnetic coupling between the spin-polarized edges. Because the interaction between spins on opposite edges increases with decreasing width, the total energy of an n-ZGNR with antiferromagnetic arrangement across opposite edges is always lower than that of a ferromagnetic arrangement if $n \leq 32$. This total energy hierarchy is maintained when external electric fields are applied. It is known that spontaneous magnetic orderings in one-dimensional and two-dimensional spin lattice models are difficult to achieve at finite temperature[24]. Spin correlation lengths comparable to nanometre-scale systems, however, are possible in practice[25–28]. Here we also expect that the spin orderings are realizable because of the large anisotropic exchange interactions between the spins in ribbons with split-gate geometry on the substrate.

We find that the ground state of the ZGNRs, including the spin degree of freedom, has a bandgap inversely proportional to the ribbon width. However, the energy splitting at $ka = \pi$ is ~0.52 eV, regardless of width, if $n \geq 8$. The states of opposite spin orientation are degenerate in all bands (Fig. 2c, left). When spins are included, the

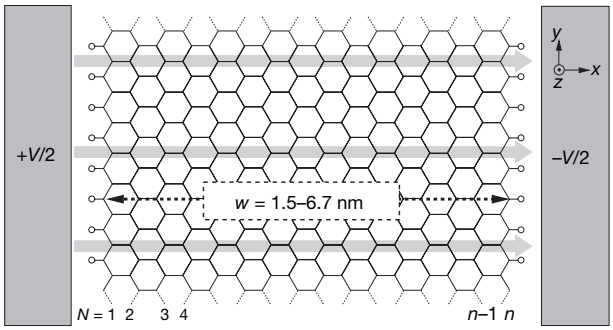

Figure 1 | Graphene nanoribbon in electric fields. Diagram of a zigzag graphene nanoribbon (ZGNR) with external transverse electric field E_{ext}. E_{ext} is applied across the ZGNR along the lateral direction (x direction) in an open-circuit split-gate configuration and is positive towards the right side. The ZGNRs are assumed to be infinite along the y direction. A small longitudinal source-drain field could be applied to generate spin-polarized currents along the y direction. Hydrogen atoms on the edges are denoted by circles. The ZGNR shown in this figure is a 16-ZGNR ($n = 16$). The width w of ZGNRs under study was in the range 1.5–6.7 nm.

[1]Department of Physics, University of California at Berkeley, Berkeley, California 94720, USA. [2]Materials Sciences Division, Lawrence Berkeley National Laboratory, Berkeley, California 94720, USA.

degeneracy between the occupied and unoccupied edge-state bands at E_F is now lifted and the edge states near E_F have dispersion along the direction of the edge with a bandwidth of ~2 eV when extended over the Brillouin zone.

With applied transverse electric fields, we find that the valence and conduction edge-state bands associated with one spin orientation close their gap, whereas those associated with the other widen theirs (Fig. 2c). So, under appropriate field strengths, the ZGNRs are forced into a half-metallic state by the applied electric field, resulting in insulating behaviour for one spin and metallic behaviour for the other. We shall defer the discussion of spin–orbit interactions later. For now, we label the gap-opening states as α-spin (shown in red in Figs 2–4) and the gap-narrowing states as β-spin (blue). In a 16-ZGNR, the bandgap associated with β-spin is completely closed by an E_{ext} of 0.1 V Å^{-1}, whereas the gap for α-spin electrons remains very large at 0.30 eV (Fig. 2c). The energy gap for the β-spin electrons changes to an indirect gap from a direct gap as E_{ext} increases, and is closed indirectly (Fig. 2c, inset). After gap closure, an electron channel near $ka = \pi$ and a hole channel near $ka = 0.75\pi$ appear at E_F, all with the same spin direction.

The half-metallicity of the ZGNRs originates from the fact that the applied electric fields induce energy-level shifts of opposite signs for the spatially separated spin-ordered edge states. Such separate and opposite energy shifts are made possible by the localized nature of the edge states around E_F. Because oppositely oriented spin states are located at the opposite sides of the ZGNR, the effect of E_{ext} on them is opposite, moving the occupied and unoccupied β-spin states closer in energy but moving the occupied and unoccupied α-spin states apart (Fig. 3). The electrostatic potential is raised on the right side and lowered on the left side as E_{ext} (>0) increases. Correspondingly, the energies for localized edge states on the right side are shifted upwards and those on the left side downwards, eventually leaving states of only one spin orientation at E_F (Fig. 3b). In a 16-ZGNR, the occupied α states and unoccupied β-spin states on the left side move downwards in energy by 19 meV and 110 meV, respectively, and occupied β-spin and unoccupied α-spin states on the right side upwards by 112 meV and 74 meV, respectively, as E_{ext} increases to 0.1 V Å^{-1} (Fig. 3c). The occupied β-spin states in the middle of a 16-ZGNR are the tails of the localized β-spin states on the right side and the unoccupied β-spin states are from the left side, so that occupied and unoccupied β-spin states in the middle of the ZGNR move oppositely to close the gap. The energies of the occupied and unoccupied α-spin states in the middle also follow movements of those of the corresponding localized states on each side, resulting in an increased gap value (Fig. 3c).

We note that the critical electric field for achieving half-metallicity in ZGNRs decreases as the width increases because the electrostatic potential difference between the two edges is proportional to the system size. For a 32-ZGNR whose width is 67.2 Å, E_{ext} = 0.045 V Å^{-1} is required to close the bandgap for the β-spin electrons (Fig. 4). Because the energy shifts of the edge states depend on the total voltage drop between the two sides, the variation of the energy gap is expected to exhibit a universal behaviour as a function of wE_{ext}, where w is the width of the ZGNR. This is seen in the inset in Fig. 4. From the calculations, the required critical field is estimated to

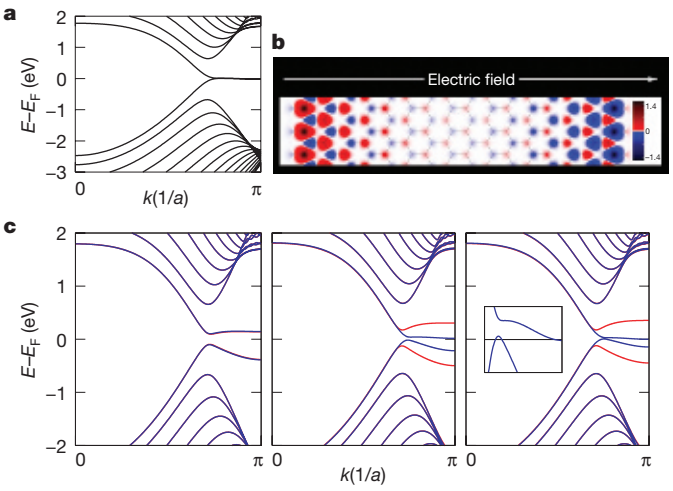

Figure 2 | Electronic structures of graphene nanoribbons. In all figures, the Fermi energy (E_F) is set to zero. **a**, The spin-unpolarized band structure of a 16-ZGNR. **b**, The spatial distribution of the charge difference between α-spin and β-spin ($\rho_\alpha(r) - \rho_\beta(r)$) for the ground state when there is no external field. The magnetization per edge atom for each spin on each sublattice is 0.43μ_B with opposite orientation, where μ_B is the Bohr magneton. The graph is the electron density integrated in the z direction, and the scale bar is in units of $10^{-2}|e|$ Å^{-2}. **c**, From left to right, the spin-resolved band structures of a 16-ZGNR with E_{ext} = 0.0, 0.05 and 0.1 V Å^{-1}, respectively. The red and blue lines denote bands of α-spin and β-spin states, respectively. Inset, the band structure with E_{ext} = 0.1 V Å^{-1} in the range $|E-E_F| < 50$ meV and $0.7\pi \le ka \le \pi$ (the horizontal line is E_F).

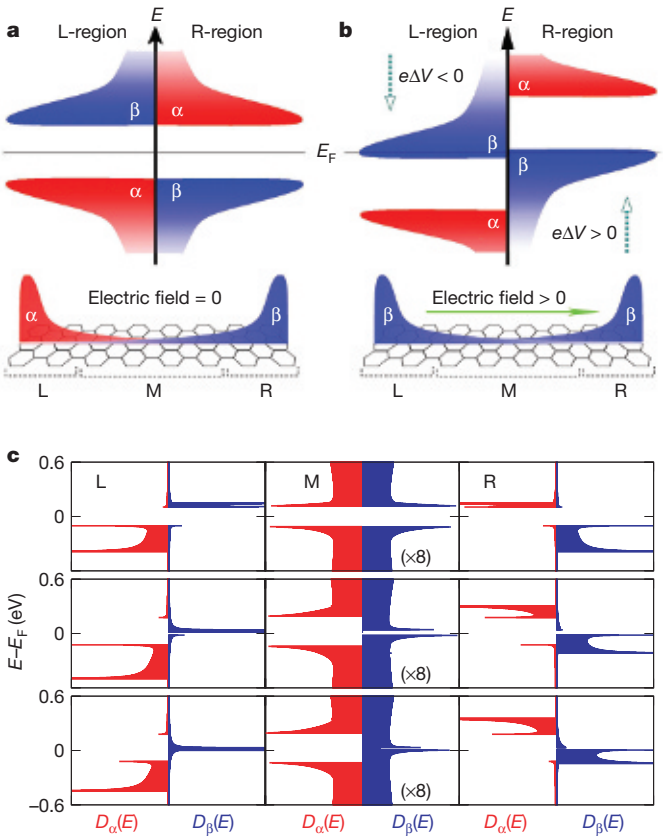

Figure 3 | Origin of half-metallicity. **a**, Schematic density-of-states diagram of the electronic states of a ZGNR in the absence of an applied electric field. Top: the occupied and unoccupied localized edge states on the left side (L-region as defined at the bottom) are the α-spin and β-spin states, respectively, and vice versa on the right side (R-region) with the same energy gap for both sides. Bottom: schematic diagram of the spatial spin distribution of the highest occupied valence band states without an external electric field. **b**, Top: with a transverse electric field, the electrostatic potential on the left edge is lowered ($e\Delta V < 0$), whereas the one on the right edge is raised ($e\Delta V > 0$). Correspondingly, the energies of the localized states at the left edge are decreased and those of the localized states at the right edge are increased. Bottom: the resulting states at E_F are only β-spin. **c**, From left to right, the local density of states of α-spins and β-spins (ordinate) of a 16-ZGNR as a function of energy (abscissa) for atoms in the L, M and R regions shown in **a**, respectively. From top to bottom, E_{ext} = 0.0, 0.05 and 0.1 V Å^{-1} respectively. The local density of states in the middle panels are enlarged eightfold for clarity. For E_{ext} = 0.1 V Å^{-1}, the van Hove singularities of the β-spin in the M and R region are above the E_F by 5 meV, and all states at E_F are of β-spin.

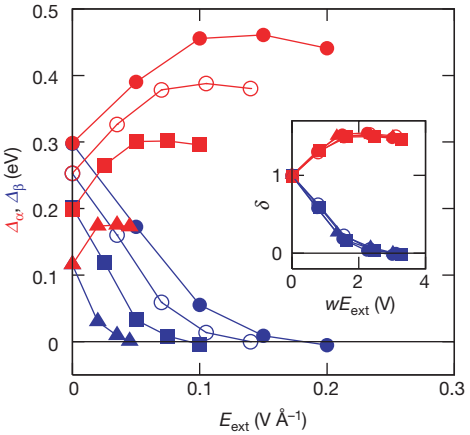

Figure 4 | Dependence of half-metallicity on system size. Δ_α (red) denotes the direct bandgap of α-spin, and Δ_β (blue) the (in)direct gap of β-spin as function of E_{ext} for the 8-ZGNR (filled circles), 11-ZGNR (open circles), 16-ZGNR (squares) and 32-ZGNR (triangles). The slope variation of Δ_α and Δ_β indicates the gap change from direct to indirect. The rescaled gaps $\delta_\alpha \equiv \Delta_\alpha(w,E_{ext})/\Delta_0(w)$ and $\delta_\beta \equiv \Delta_\beta(w,E_{ext})/\Delta_0(w)$ for the various widths collapse to a single function of wE_{ext} as shown in the inset, where $\Delta_\alpha(w,E_{ext})$ and $\Delta_\beta(w,E_{ext})$ are the bandgaps for the α-spins and β-spins, respectively, of the ZGNR with a width of w in E_{ext} ($\neq$0), and $\Delta_0(w) \equiv \Delta_\alpha(w,E_{ext}=0) = \Delta_\beta(w,E_{ext}=0)$.

be 3.0 (V)/w(Å). To establish half-metallicity, the relevant energy scale is given by the field-induced energy shift, and its magnitude is in the order of 100 meV. Thus the small magnitude of spin–orbit interaction (4–6 meV) in carbon atoms[29,30] would not change the half-metallic nature of the ZGNRs but would function in determining the spatial direction (normal direction with respect to the ribbon plane) of spin up and down in the ZGNRs[29].

Because edges are inevitably susceptible to defects, we have examined the robustness of the predicted half-metallicity to edge defects. Our calculations show that the system remains purely of one spin type at E_F in the presence of different types and concentrations of defects. Results on 8-ZGNRs with three different kinds of defect (dangling bonds, vacancies and Stone–Wales defects at 6–12% defect concentration per edge) are presented in Supplementary Fig. 1, confirming that the predicted half-metallicity is indeed robust.

Another consideration is that, when in the half-metallic state the ZGNRs are in a transverse electric field, the current-carrying electrons moving from the source to the drain in the longitudinal direction would experience an effective magnetic field due to spin–orbit interactions[6,7] and the spins are expected to rotate. However, we find that the resulting extremely weak effective magnetic fields are parallel to the spatial spin direction (z direction in Fig. 1) already determined by the intrinsic spin–orbit interactions of carbon atoms. Suppose that we have the β-spin electrons moving with velocity $\mathbf{v} = v\hat{y}$ in $\mathbf{E} = E_{ext}\hat{x}$, the effective magnetic field exerted on the β-spin electrons would be $\mathbf{B_{eff}} = (ev\hbar/4mc^2)E_{ext}\hat{z}$, where $\hbar$ is the Planck constant, m is the mass of an electron, e is the charge on an electron, and c is the speed of light. At a critical electric field of 0.045 V Å^{-1} for a 32-ZGNR, the estimated energy for spin–orbit coupling due to E_{ext} is only 1.1×10^{-4} meV. We also find that, as a result of the energy gap asymmetry for each spin, there is no spin precession even when the direction of E_{ext} is tilted or when the spatial spin direction is altered by spin–orbit interaction arising from the substrate. So, the spatial spin direction once determined would not change even if a strong transverse electric field were applied. This implies that, if we change the direction of E_{ext}, the spin polarity of the carriers at E_F of the half-metallic ribbon will be reversed because the induced potentials at the edges change their signs. Hence, under these conditions, the half-metallic nature is robust even though a transverse electric field is applied, and spin-polarized current should be obtained in a transport experiment with split gates.

Received 24 March 2006; accepted 16 August 2006.

1. de Groot, R. A., Mueller, F. M., van Engen, P. G. & Buschow, K. H. J. New class of materials: half-metallic ferromagnets. *Phys. Rev. Lett.* **50,** 2024–2027 (1983).
2. Park, J-H. *et al.* Direct evidence for a half-metallic ferromagnet. *Nature* **392,** 794–796 (1998).
3. Wolf, S. A. *et al.* Spintronics: A spin-based electronics vision for the future. *Science* **294,** 1488–1495 (2001).
4. Fang, C. M., de Wijs, G. A. & de Groot, R. A. Spin-polarization in half-metals. *J. Appl. Phys.* **91,** 8340–8344 (2002).
5. McEuen, P. L., Fuhrer, M. S. & Park, H. Single-walled carbon nanotube electronics. *IEEE Trans. Nanotechnol.* **1,** 78–85 (2002).
6. Murakami, S., Nagaosa, N. & Zhang, S-C. Dissipationless quantum spin current at room temperature. *Science* **301,** 1348–1351 (2003).
7. Sinova, J. *et al.* Universal intrinsic spin Hall effect. *Phys. Rev. Lett.* **92,** 126603 (2004).
8. Berger, C. *et al.* Ultrathin epitaxial graphite: 2D electron gas properties and a route toward graphene-based nanoelectronics. *J. Phys. Chem. B* **108,** 19912–19916 (2004).
9. Novoselov, K. S. *et al.* Two-dimensional gas of massless Dirac fermions in graphene. *Nature* **438,** 197–200 (2005).
10. Zhang, Y., Tan, Y-W., Stormer, H. L. & Kim, P. Experimental observation of the quantum Hall effect and Berry's phase in graphene. *Nature* **438,** 201–204 (2005).
11. Berger, C. *et al.* Electronic confinement and coherence in patterned epitaxial graphene. *Science* **312,** 1191–1196 (2006).
12. Fujita, M., Wakabayashi, K., Nakada, K. & Kusakabe, K. Peculiar localized state at zigzag graphite edge. *J. Phys. Soc. Jpn.* **65,** 1920–1923 (1996).
13. Nakada, K., Fujita, M., Dresselhaus, G. & Dresselhaus, M. S. Edge state in graphene ribbons: nanometer size effect and edge shape dependence. *Phys. Rev. B* **54,** 17954–17961 (1996).
14. Wakabayashi, K., Fujita, M., Ajiki, H. & Sigrist, M. Electronic and magnetic properties of nanographite ribbons. *Phys. Rev. B* **59,** 8271–8282 (1999).
15. Miyamoto, Y., Nakada, K. & Fujita, M. First-principles study of edge states of H-terminated graphitic ribbons. *Phys. Rev. B* **59,** 9858–9861 (1999).
16. Kobayashi, Y., Fukui, K-I., Enoki, T., Kusakabe, K. & Kaburagi, Y. Observation of zigzag and armchair edges of graphite using scanning tunneling microscopy and spectroscopy. *Phys. Rev. B* **71,** 193406 (2005).
17. Niimi, Y. *et al.* Scanning tunneling microscopy and spectroscopy of the electronic local density of states of graphite surfaces near monoatomic step edges. *Phys. Rev. B* **73,** 085421 (2006).
18. Okada, S. & Oshiyama, A. Magnetic ordering in hexagonally bonded sheets with first-row elements. *Phys. Rev. Lett.* **87,** 146803 (2001).
19. Lee, H., Son, Y-W., Park, N., Han, S. & Yu, J. Magnetic ordering at the edges of graphitic fragments: Magnetic tail interactions between the edge-localized states. *Phys. Rev. B* **72,** 174431 (2005).
20. Son, Y-W., Ihm, J., Cohen, M. L., Louie, S. G. & Choi, H. J. Electrical switching in metallic carbon nanotubes. *Phys. Rev. Lett.* **95,** 216602 (2005).
21. Soler, J. M. *et al.* The SIESTA method for *ab intio* order-*N* materials simulation. *J. Phys. Condens. Matter* **14,** 2745–2779 (2002).
22. Perdew, J. P. & Zunger, A. Self-interaction correction to density-functional approximations for many-electron systems. *Phys. Rev. B* **23,** 5048–5079 (1981).
23. Lieb, E. H. Two theorems on the Hubbard model. *Phys. Rev. Lett.* **62,** 1201–1204 (1989).
24. Mermin, N. D. & Wagner, H. Absence of ferromagnetism or antiferromagnetism in one- or two-dimensional isotropic Heisenberg models. *Phys. Rev. Lett.* **17,** 1133–1136 (1966).
25. Gambardella, P. *et al.* Ferromagnetism in one-dimensional monatomic metal chains. *Nature* **416,** 301–304 (2002).
26. Dorantes-Dávila, J. & Pastor, G. M. Magnetic anisotropy of one-dimensional nanostructures of transition metals. *Phys. Rev. Lett.* **81,** 208–211 (1998).
27. Vindigni, A., Rettori, A., Pini, M. G., Carbone, C. & Gambardella, P. Finite-sized Heisenberg chains and magnetism of one-dimensional metal systems. *Appl. Phys. A* **82,** 385–394 (2006).
28. Delin, A., Tossati, E. & Weht, R. Magnetism in atomic-size palladium contacts and nanowires. *Phys. Rev. Lett.* **92,** 057201 (2004).
29. Yao, Y., Ye, F., Qi, X-L., Zhang, S-C. & Fang, Z. Spin-orbit gap of graphene. Preprint at <http://arxiv.org/abs/cond-mat/0606350> (2006).
30. Min, H. *et al.* Intrinsic and Rashba spin-orbit interactions in graphene sheets. Preprint at <http://arxiv.org/abs/cond-mat/0606504> (2006).

Supplementary Information is linked to the online version of the paper at www.nature.com/nature.

Acknowledgements We thank J. Neaton, F. Giustino, I. Souza, C. H. Park and H. J. Choi for discussions. This research was supported by the National Science Foundation (NSF) and by the Director, Office of Science, Office of Basic Energy Science, Division of Material Sciences and Engineering, US Department of Energy (DOE). Computational resources have been provided by the NSF at the National Partnership for Advanced Computational Infrastructure and by the DOE at the National Energy Research Scientific Computing Center.

Author Information Reprints and permissions information is available at www.nature.com/reprints. The authors declare no competing financial interests. Correspondence and requests for materials should be addressed to S.G.L. (sglouie@berkeley.edu).

CORRIGENDUM

doi:10.1038/nature05274

Happy centenary, photon

Anton Zeilinger, Gregor Weihs, Thomas Jennewein & Markus Aspelmeyer

Nature 433, 230–238 (2005)

In the legend to Figure 1, the experiment shown was wrongly attributed to Clauser. The legend should have read 'Principle of Grangier, Roger and Aspect's experiment…(ref. 10)'. In contrast, the Clauser experiment (ref. 4) involved one beam splitter on each side with detectors in each of the resulting four output ports. Four characteristic correlations were measured. In both the Clauser (ref. 4) and the Grangier, Roger and Aspect (ref. 10) experiments the observed correlations cannot be explained via classical light fields, but can easily be understood by assuming single photons that can only be detected once behind a beam splitter.

CORRIGENDUM

doi:10.1038/nature05641

The receptors and coding logic for bitter taste

K. L. Mueller, M. A. Hoon, I. Erlenbach, J. Chandrashekar, C. S. Zuker & N. J. P. Ryba

Nature 434, 225–229 (2005)

C.S.Z., N.J.P.R., K.L.M. and M.A.H. filed a patent application relevant to this work on 10 September 1999 (patent number US6558910), which should therefore have been declared as a competing financial interest.

CORRIGENDUM

doi:10.1038/nature05686

Half-metallic graphene nanoribbons

Young-Woo Son, Marvin L. Cohen & Steven G. Louie

Nature 444, 347–349 (2006)

In Fig. 2b of this Letter, the contour values were incorrectly normalized. The maximum and minimum values of ± 1.4 in the scale bar in Fig. 2b should read ± 36.6. This error does not affect any of our results. We thank E. Rudberg for pointing out this error.

CORRIGENDUM

doi:10.1038/nature05606

The prolyl isomerase Pin1 regulates amyloid precursor protein processing and amyloid-β production

L. Pastorino, A. Sun, P.-J. Lu, X. Z. Zhou, M. Balastik, G. Finn, G. Wulf, J. Lim, S.-H. Li, X. Li, W. Xia, L. K. Nicholson & K. P. Lu

Nature 440, 528–534 (2006)

During editing to meet *Nature*'s limits on length, we removed a reference to an earlier paper[1] reporting that the prolyl isomerase Pin1 promotes production of Alzheimer's amyloid-β (Aβ) from β-cleaved amyloid precursor protein (APP). That paper reported that Pin1 did not bind to full-length APP, but rather to the phosphorylated Thr 668–Pro motif of the carboxy-terminal C99 fragment of APP; Aβ production in Pin1-knockout mice was reduced only from this fragment.

1. Akiyama, H., Shin, R. W., Uchida, C., Kitamoto, T. & Uchida, T. Prolyl isomerase Pin1 facilitates production of Alzheimer's amyloid-β from β-cleaved amyloid precursor protein *Biochem. Biophys. Res. Commun.* 336, 521–529 (2005).

CORRIGENDUM

doi:10.1038/nature05608

Human embryonic stem cell lines derived from single blastomeres

Irina Klimanskaya, Young Chung, Sandy Becker, Shi-Jiang Lu & Robert Lanza

Nature 444, 481–485 (2006); doi:10.1038/nature05142 and *Nature* 444, 512 (2006); doi:10.1038/nature05366

The last sentence of the penultimate paragraph of this Letter should read "Notably, individual morula (8–16 cell)-stage blastomeres have not been shown to have the intrinsic capacity to generate a complete organism in most mammalian species." (see refs 1 and 2).

1. Moore, N. W., Adams, C. E. & Rowson, L. E. A. Developmental potential of single blastomeres of the rabbit egg. *J. Reprod. Fertil.* 17, 527–531 (1968).
2. Willadsen, S. M. The developmental capacity of blastomeres from four and eight-cell sheep embryos. *J. Embryol. Exp. Morph.* 65, 165–172 (1981).